

# 3 PF-AR

## 3-1 Summary of Machine Operation

Commissioning following the PF-AR upgrade project was successfully completed in January 2002. After vacuum scrubbing with the beam and fine-tuning of the machine, users' runs started at the beginning of April. The operation statistics for FY2002 are summarized in Table 1. The total operation time was 4667 hours, with 3726 hours (79.8%) for user runs. Machine study and tuning time was 778 hours (16.7%), failure time was 78.5 hours (1.7%). The history of the total operation time of the PF-AR ring is shown in Fig. 1. Six periods of 5.0-GeV operation dedicated to coronary angiography were successfully performed in FY2002. A new beamline NW2 for pulsed X-ray experiments was constructed and is now in the commissioning stage. The first beamline in the northwest experimental hall, NW12, dedicated to structural biology was also constructed with an in-vacuum type tapered undulator.

Although the beam lifetime was largely improved after the vacuum scrubbing, we still had many issues to solve: the maximum available beam current, the stability of the close orbit, sudden changes in the beam lifetime etc., which are all long-standing problems, and we have been making every effort to improve them. One of the most serious problems was the deterioration of the injection rate at a certain beam current. This phenomenon limited the maximum available current to about 45 mA. In order to reduce this effect, which seems to be caused by a wake field excited in the RF cavities by the beam already

stored in the ring, we changed the injection energy from 2.5 GeV to 3.0 GeV considering that the higher beam energy gives higher thresholds of instabilities, as described in the following sections. Beam injection in the routine operation became easier, and the maximum stored current was largely improved as well. At present, the typical initial beam current in routine operation is 55 mA and the lifetime at this current is 15 hours. A slow orbit drift that depends on the beam current is observed without an orbit feedback system. Before the upgrading project, the global orbit feedback system was not effective because of the lack of reliability of the beam position monitor (BPM) system. Since renewal of the BPM electrodes and multiplexer relays in the upgrading project, making the system fast and reliable, we are now able to correct the orbit accurately every 20 seconds. Examples of the machine developments were mentioned briefly here, and some of them will be reported in detail in the following sections.

Although many problems were already resolved after the upgrading project, we still have several issues to solve urgently. These are summarized below.

1. The temperature in the PF-AR tunnel affects the operation of the machine. As reported in the following section, we sometimes encounter a situation in that the only solution for sudden beam loss during acceleration is to change the tunnel temperature. We have to investigate the real origin of the phenomenon.

2. Sudden changes in the beam lifetime is one of the serious problems of the PF-AR. Sometimes the lifetime becomes short suddenly during users' runs. The recovery from the short lifetime depends on the circumstances. (Sometimes it recovers, sometimes does not.) It seems that the frequency of the phenomena is becoming lower. We do not know its source and the means to cure it yet though we have been making efforts to solve the problem.

3. The present value of the emittance (290 nm-rad) is not satisfactory. We have been making efforts to find a stable operating point that gives the optimum emittance of 160 nm-rad.

Table 1 Operation statistics of the PF-AR in FY2002.

Operation Time	4667.0 (hours)	100.0%
SR Experiment	3726.0 (hours)	79.8%
Beam Development	778.5 (hours)	16.7%
Failure	78.5 (hours)	1.7%
Miscellaneous	84.0 (hours)	1.8%

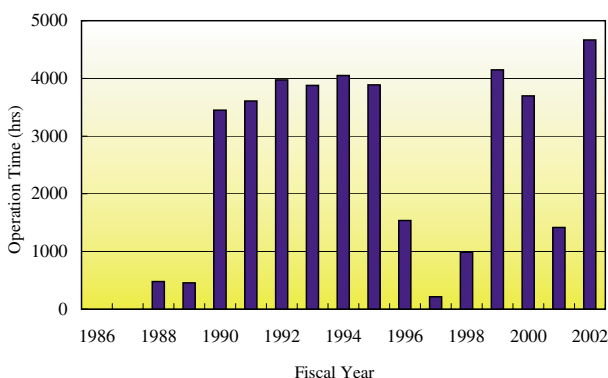


Figure 1 Operation time history of the PF-AR.

## 3-2 3-GeV Injection

Since September 2002, the injection energy of PF-AR has been increased from 2.5 GeV to 3.0 GeV. As a result of this change, the stored current during the user runs has improved from 40 mA to about 55 mA. We present the motivation for, and the accomplishment of the 3-GeV injection project in this section.

In case of the 2.5-GeV injection, the maximum stored current was limited to 45 mA even under good conditions.

There were also difficulties in the injection tuning during daily operation. As shown in Fig. 2, the injection rate drastically decreased from about 0.9 mA/s to 0.25 mA/s at a stored current of 35 mA. We, therefore, fixed the initial beam current for user runs at 40mA since this was the maximum current we could store without careful tunings which lengthened injection time. We were aware that the cause of these phenomena was beam instabilities. In order to suppress these, we thought a higher energy injection would be effective. Because the design energy of the beam transport line and the injection system (kicker and septum magnets) are 3.0 GeV, 3-GeV injection can be achieved without renewal of the hardware.

We made a preparatory machine study on June 10, 2002. As the tuning of the injector LINAC to produce a stable 3-GeV electron beam had been finished in advance, we could lead 3-GeV electrons to the ring at once and store a beam current of 65 mA in a few hours after the study began. The beam instability was well suppressed and the injection rate was kept over about 0.8 mA/s during injection as shown in Fig. 3. With machine tuning of the acceleration, we could achieve a stored current of 52 mA at 6.5 GeV and the study finished successfully. The problem was, however, the rise of the vacuum pressure and the temperature of the beam duct. For example, the temperature of the joint chamber between the normal duct and the RF cavity went up to over 100°C for

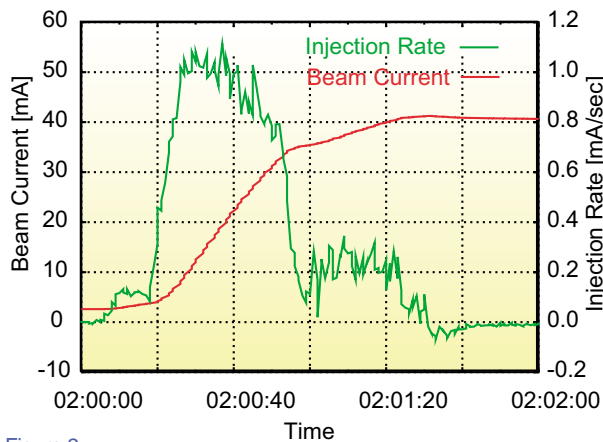


Figure 2  
Typical injection pattern at 2.5 GeV.

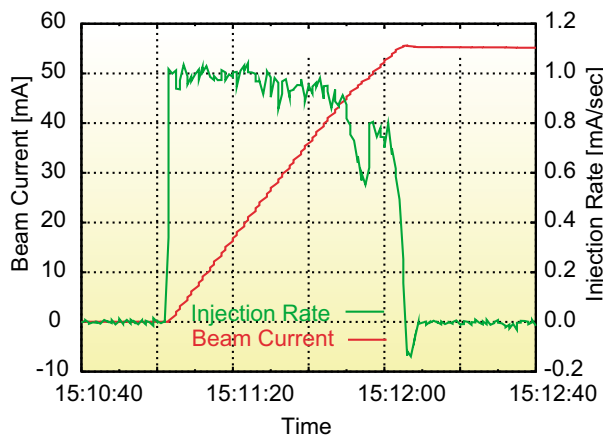


Figure 3  
Typical injection pattern at 3.0 GeV.

a beam current of 50 mA at 6.5 GeV.

Due to the success of the machine study, the injection energy was changed from 2.5 GeV to 3.0 GeV during the commissioning in September 2002. For user operation, the initial beam current after the injection was fixed at 50 mA. With improvement of the vacuum pressure, the initial beam current was increased. For the user run in February 2003, the initial beam current was about 55 mA and the beam lifetime was 15 hours. At 6.5 GeV, the maximum stored current is about 60 mA due to the limitation of RF power.

### 3-3 Orbit Stabilization

In the PF-AR, a slow orbit drift is observed depending on the beam current during the user operation mode. The typical initial stored current is 55 mA, and the current decreases to 30 mA at the end of an 8-hour operation shift. Thermal deformation of the magnet poles and the vacuum chambers generates a reproducible closed orbit distortion (COD), and rms values of the orbit drift in the horizontal and vertical directions are 85  $\mu\text{m}$  and 63  $\mu\text{m}$ ,

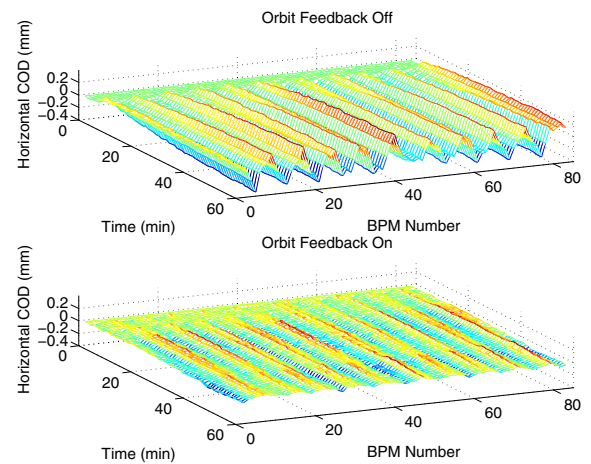


Figure 4  
Horizontal orbit fluctuations with and without global orbit feedback.

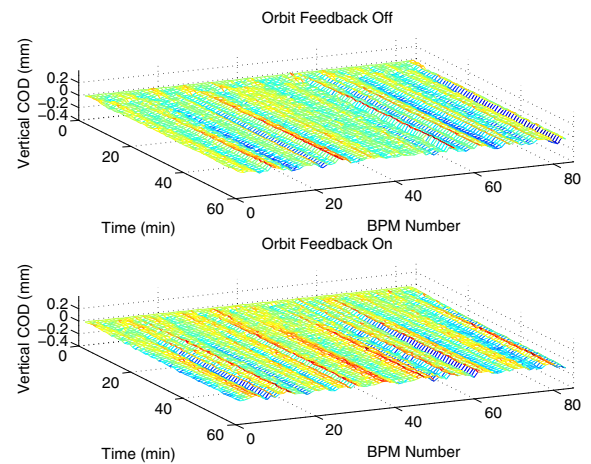


Figure 5  
Vertical orbit fluctuations with and without global orbit feedback.

respectively.

In order to suppress this orbit distortion, we have prepared a global orbit feedback system which continuously corrects the COD with a period of 20 s. With the new system, the rms values of the horizontal and vertical orbit drift were effectively reduced to 16  $\mu\text{m}$  and 29  $\mu\text{m}$ , respectively. Comparisons of the horizontal and vertical orbit drift with and without the feedback are shown in Figs. 4 and 5.

### 3-4 Vacuum System

The improvements in the beam lifetime and the average pressure of PF-AR from January 2002 to February 2003 are shown in Fig. 6. The electron-beam lifetime  $I\tau$  grew up to 50 A·min, 7 times longer than that of the former PF-AR. The reason for the deterioration of the beam lifetime and the average pressure at an integrated current of 80 A·h was the installation of a new insertion device at NW12 in the summer of 2002. After the injection energy

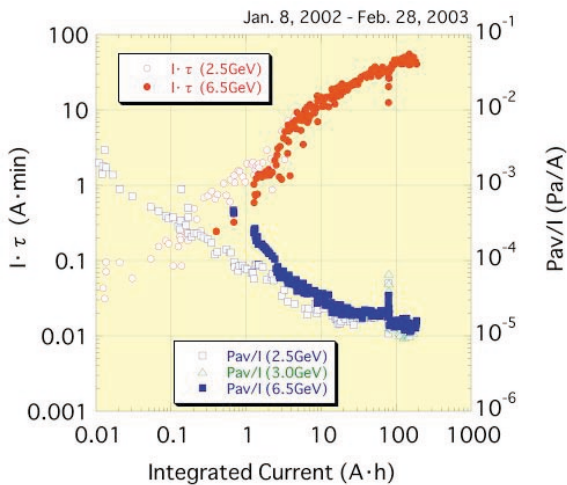


Figure 6 Progress of the beam ducts cleaning and growth of the beam lifetime.

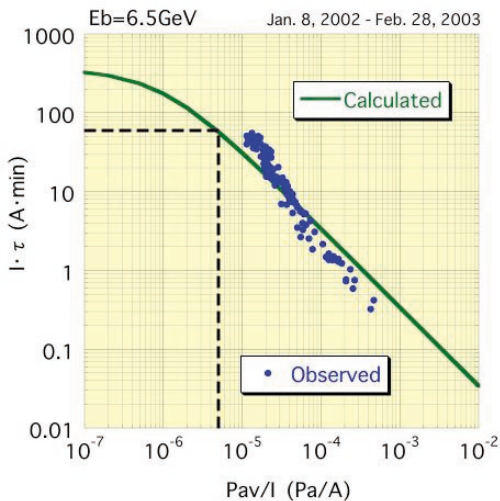


Figure 7 Relationship between the pressure and the lifetime.

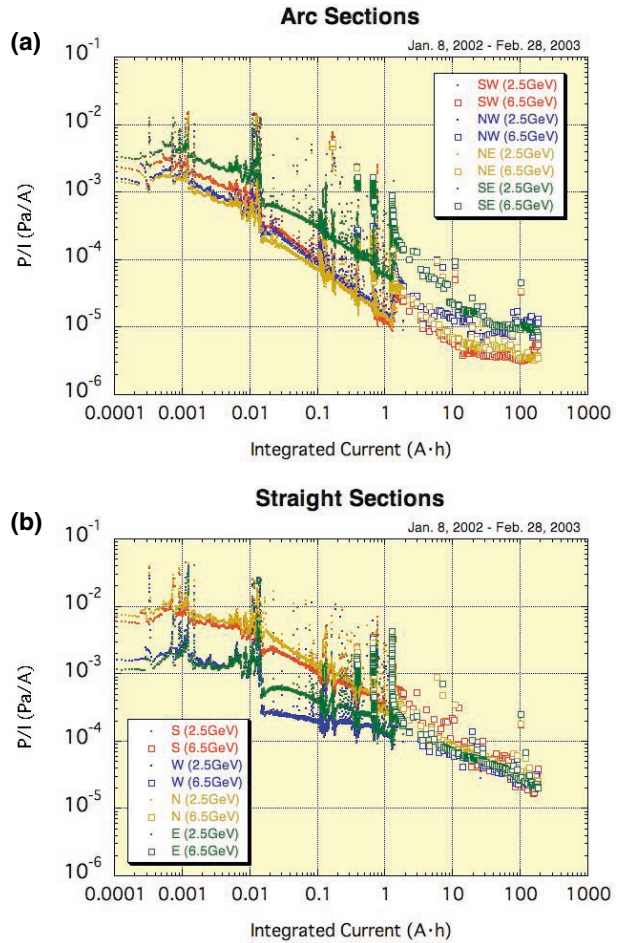


Figure 8 Progress of the beam ducts cleaning in the arc sections (a) and the straight sections (b).

was changed to 3.0 GeV from 2.5 GeV in September 2002, the initial stored current has increased gradually, and currently reaches 55 mA. Operators inject the beam three times a day on schedule if neither a serious lifetime drop nor a sudden beam dump happens. Although the frequency of sudden lifetime drops is decreasing, this remains one of the unsolved problems in the PF-AR operation.

While the growth of the beam lifetime becomes slower, even longer lifetimes are expected if a lower pressure can be achieved. As shown in Fig. 7, the relationship between the ring average pressure and the beam lifetime indicates that the lifetime is still being limited by the beam-gas scattering (inversely proportional region) and not by Touschek effects (flat region).

Figures 8(a) and 8(b) show the progress of the vacuum ducts cleaning in the arc sections and the straight sections, respectively. It is clear that the pressures in the straight sections are the dominant factors for the average ring pressure. Therefore, the reinforcement of the pumping ability in the straight sections will be an effective way to lower the average ring pressure.

### 3-5 Temperature Control in the Ring Tunnel

The operation of the PF-AR ring has become more and more stable after the upgrade project. We sometimes suffer, however, from beam loss during the acceleration process. By adjustment of the machine parameters relating to the magnets and the RF system, we cannot improve the situation when the problem is severe. In such cases, the only solution is to change the settings of the ring-tunnel temperature. It is empirically clear that the machine condition is strongly affected by the temperature in the tunnel, although the reason is unclear.

Air-conditioning for the AR tunnel is separately controlled at four areas, north, east, south and west. At present, target values for the temperature are set at 27~28°C for the west area and 24°C for the other areas. These temperatures were chosen empirically from the optimum machine condition for stable acceleration.

The temperature monitoring system had been reinforced during the summer shutdown of 2002, until then only four thermometers were available in the AR tunnel. Now eighteen thermometers are available and the detailed temperature distribution can be recorded continuously. Figure 9(a) shows the observed temperatures in the AR tunnel during the operation period of Autumn 2002. The problems are as follows: 1) poor stability, 2)

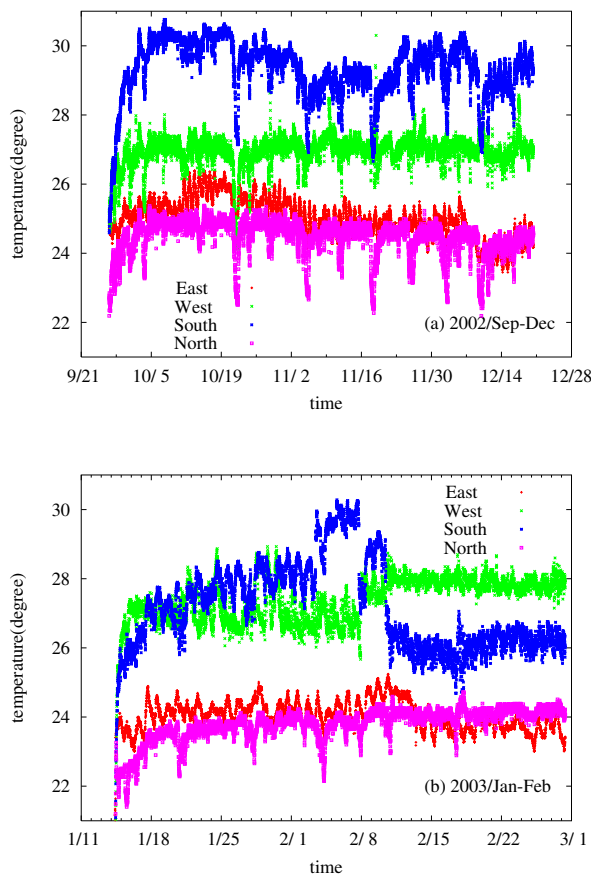


Figure 9 Temperature in the AR tunnel for 2002 Autumn period (a) and 2003 winter period (b). Red, green, blue and pink points show temperature in the East, West, South and North areas, respectively.

higher temperatures in south and west areas, 3) over-cooling during short shutdowns or low energy operation, and 4) influence of atmospheric temperature. A common source of these problems is insufficient cooling power to control the temperature at the set value.

In order to stabilize the temperature and the beam operation, we have performed following tasks: 1) adjustment of the setting in the west area, 2) blocking of air current directly blowing the RF cavities by obstacle plates installed in front of outlets of the air conditioner, 3) shutting off warm water for the south air-conditioner (it had leaked due to superannuation of a two-way valve), 4) to take care of over-cooling during short shutdown or low-energy operation, and 5) investigation of the air-conditioning system. Although problems still remain, the temperature condition in AR tunnel has improved as can be seen in Fig. 9(b), which shows temperatures during the first operation period of 2003. The temperature became stable especially for the latter half of February. It is anticipated that better temperature conditions will be found and better beam operation will be established in the near future after more systematic investigations.

### 3-6 Transverse Sawtooth Instability

As the stored beam current increases during injection, a curious phenomenon called transverse sawtooth instability is observed in the PF-AR. As shown in Fig. 10, a betatron oscillation induced by an injection error continues to grow over several milliseconds after initial damp-

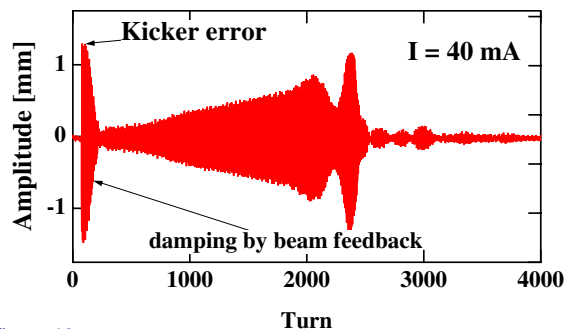


Figure 10 Transverse (horizontal) sawtooth instability observed at 3-GeV injection.

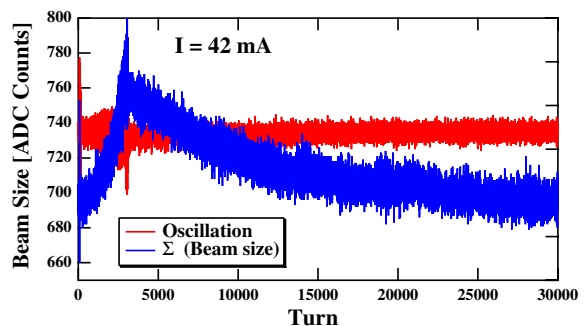


Figure 11 Variation of beam size (blue) superimposed on the dipole oscillation.

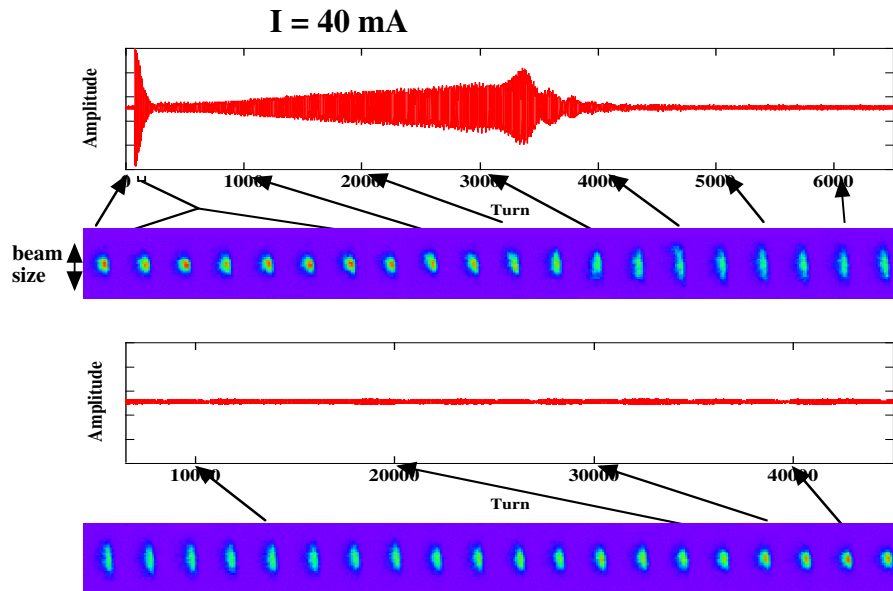


Figure 12  
Horizontal beam profiles taken by the streak camera and the horizontal oscillation are shown as a function of turn number.

ing due to beam feedback, before finally being damped rapidly. This instability was first observed at 2.5-GeV injection, and was assumed to be closely related to the deterioration of injection rate at high current. At 3-GeV injection, a similar instability was also observed although a clear change of the injection rate did not occur. We found that the feedback which damps the betatron oscillation also excites the instability, octupole fields are effective in suppressing the instability, and also that a longitudinal bunch shape seemed to influence the sawtooth instability.

Beam size was deduced from a measurement of quadrupole moment of the beam. The turn-by-turn change of the beam size is shown in Fig. 11 superimposed on the variation of the sawtooth-instability amplitude. As the amplitude of the betatron oscillation grows, the beam size also grows monotonically. When the betatron oscillation reaches maximum amplitude, the beam size also reaches its maximum value. Recovery of the beam size is slow, and the size returns to its initial value on the time scale of the radiation damping time. The beam size was directly measured using a streak camera. Figure 12 shows horizontal beam profiles sampled by the streak camera with bunch oscillations. We have confirmed that the horizontal beam size and the oscillation amplitude grow together, and that the size shrinks slowly after the oscillation fully damps, as observed by measurement of the quadrupole moment.

We have also observed with the streak camera that the head and the tail of a bunch oscillate individually like a strong head-tail instability. The different oscillations at the head and the tail of a bunch may influence the detection of the bunch oscillation in the beam feedback. We plan to clarify the detailed mechanism of the sawtooth instability with a computer simulation which includes the internal bunch structure.

### 3-7 Bunch Lengthening and Impedance of Vacuum Components

The bunch-length was measured as a function of the stored bunch current. The bunch length was deduced from two frequency components in the beam spectrum. Even though the bunch shape changes, the rms value of the bunch length can be detected in real time. A comparison of the present measurement with the previous measurement performed in 1998 for the AR before the upgrade project is shown in Fig. 13. For the old AR, the bunch length increased slowly up to a bunch current of 8 mA, and then an abrupt increase of 50% occurred. This jump in the bunch length indicates a clear instability threshold. In the present measurement, the relative bunch lengthening was smaller than that of the old ring at the same bunch current. The data for low current were fitted with a calculation based on the potential-well distortion model. The effective longitudinal impedances for the

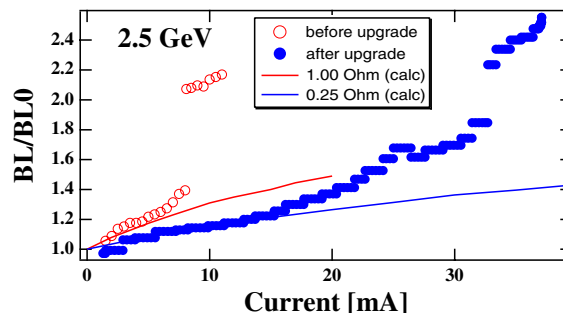


Figure 13  
Comparison of bunch lengthening at 2.5 GeV with that of AR before upgrade. Bunch length (BL) measured as a ratio to the bunch length at zero current (BL0) is plotted in the figure.

present and the old AR were estimated to be  $0.25 \Omega$  and  $1.0 \Omega$ , respectively. The bunch length of the present ring gradually deviated from calculation above 14 mA. We observed a jump at a bunch current of 30 mA. This specific current is much higher than that observed for the old ring.

During the upgrade project, all vacuum components except for the RF cavities and some insertion devices were replaced by newly designed ones. In the old vacuum system, a number of bellows without any RF shielding were installed. The total impedance of the unshielded bellows can be estimated to be  $0.62 \Omega$  using their geometric parameters. The reduction of the effective impedance obtained from the bunch length measurement was  $0.75 \Omega$ . We conclude that the greater part of the impedance change is caused by the replacement of the old bellows with well shielded ones.

### 3-8 Detection of Wake Field Using the Test-Bunch Method

Some curious phenomena have been observed during injection. One of them was the sudden deterioration of the injection rate at 2.5-GeV injection. Such deterioration of the injection rate did not appear after the injection energy was raised to 3.0 GeV. Lots of experimental facts on the beam injection suggest that the wake field excited by the stored beam affects the motion of the injected beam. We have tried to detect the wake field using a test-bunch method. In the test-bunch method, two bunches, the "main bunch" and "test bunch" are injected. The bunch

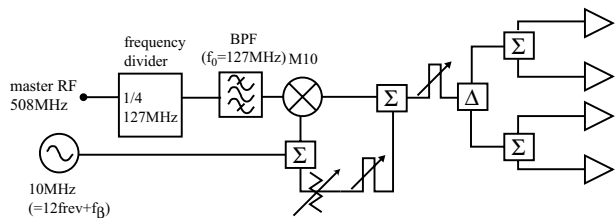


Figure 14  
Block diagram of the system for main bunch excitation. An excitation signal is composed from a sinusoidal signal at the frequency of  $f_{RF}/n$  ( $n=2,4,8$ ) and betatron frequency.

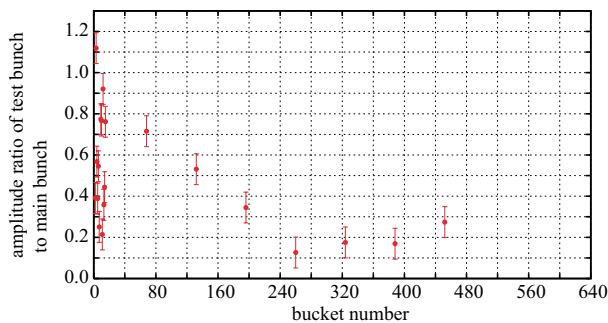


Figure 15  
Amplitude ratio of test bunch to main bunch for whole the ring. The beam energy was 3.0 GeV. The bunch current of main bunch and test bunch were 2.0 mA and 0.2 mA, respectively.

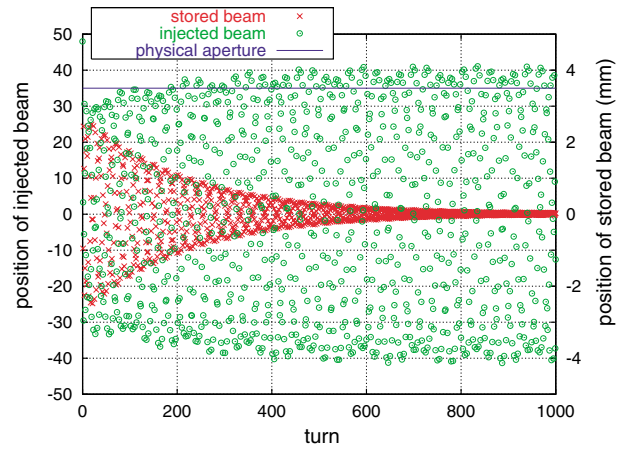


Figure 16  
Result of the numerical simulation. Solid line indicates a physical aperture by a septum magnet.

current of the test bunch is small compared with that of the main bunch. When an oscillation of the main bunch is excited artificially, the wake field induced by the main bunch affects the motion of the test bunch. From the motion of the test bunch, information on the wake field can be obtained. In this method, oscillation of the main bunch is excited but the test bunch must not be affected by the excitation. Figure 14 is a block diagram of the system to excite the main bunch oscillation [1].

Figure 15 shows the ratio of the amplitude of the test bunch to that of the main bunch obtained in the horizontal direction at an energy of 3.0 GeV. The abscissa indicates the bucket number of the test bunch. The ratios of 20 buckets after the main bunch are scattered, but they decrease gradually on the whole. From the experimental result and an analytic calculation on the motion of bunches, we have estimated the wake potential. The estimated wake potential is consistent with that obtained using the electro-magnetic calculation code MAFIA within a factor of 2.

In order to investigate the behavior of the stored beam and the injected beam when the stored beam excites a wake field and affects the injected beam, we have carried out a numerical simulation. In the simulation, each beam is modeled by a point charge. Particles are focused linearly in the magnets and kicked by the feedback damper and by the wake field. The result is shown in Fig. 16. Although the main bunch oscillation is damped in about 200 turns, the amplitude of the injected beam grows over a few hundred turns due to the wake field excited by the stored beam. The simulation also indicates that the behavior of the injected beam depends on the initial conditions of the injected beam and stored beam. As a next plan, we are going to investigate the motion of the beam injected in the bucket next to that of the stored beam at a current of about 35 mA.

#### References

- [1] T. Fujita *et al.*, to be published in *Proc. Particle Accelerator Conference 2003*.

### 3-9 Construction of SR Monitor

Since monitoring the beam profile or beam size using synchrotron radiation improves the efficiency of the commissioning of the ring, we decided to construct a new synchrotron radiation (SR) beam monitor system.

The visible part of the SR beam radiated from the NW5-bending magnet is extracted by a water-cooled beryllium mirror. The SR beam is then split into two beam-lines, and relayed to the end of the optical path by several mirrors. The total length of the optical path is about 19 m and is enclosed by aluminum tubes and boxes (not evacuated) to reduce the turbulence effect of the air. The outline of the arrangement of optical paths is shown in Fig. 17. At the end of optical path, the SR monitor hut is set on the ground floor. A conventional beam profile monitor based on a focusing system [1] is set at the end of beam line No.1. A typical image of the beam profile is shown in Fig. 18. To observe the thermal deformation of the beryllium extraction mirror, we set a Hartmann-screen type wavefront sensor next to the extraction mirror [2].

An SR interferometer [3] is used to monitor the beam size. Two independent SR interferometers are set at the end of branch beamline No.2 for measurements of both vertical and horizontal beam sizes. We use an aplanatic Fizeau type double-slit SR interferometer for the horizontal beam size measurement as illustrated in Fig. 19. For the vertical beam size measurement, we use a nonaplanatic

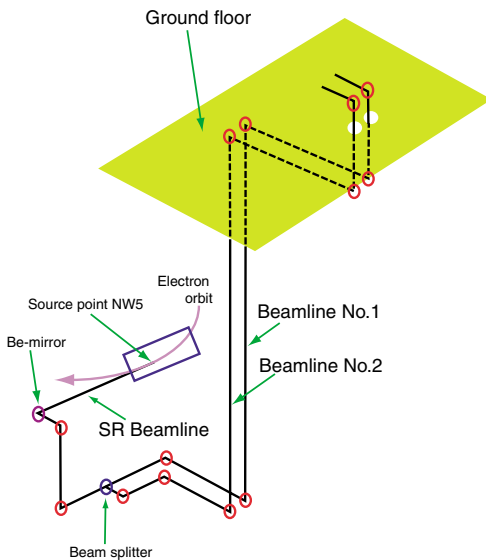


Figure 17  
Outline of optical path. Circles denote flat mirrors.



Figure 18  
An example of observed beam profile taken at 50 mA, 6.5 GeV.

Michelson type SR interferometer as illustrated in Fig. 20. With this configuration of the SR interferometer, the spatial frequency of the interferogram is a function of the beam separation ( $D_1$ ) and the modulation of the interferogram is a function of the double slit separation ( $D_2$ ) [3]. Since we can choose a fixed small separation of  $D_1$ , and a movable large separation of  $D_2$ , we can easily measure the modulation of the interferogram in the vertical small beam size measurement. Using a Gaussian beam profile approximation, we can measure the RMS beam size from one measurement of visibility from an interferogram, which is measured at a fixed separation of the double slit. After processing of the interferogram, the results are displayed on a CRT panel as shown in Fig. 21. The interferogram, best fit curve and beam size trend

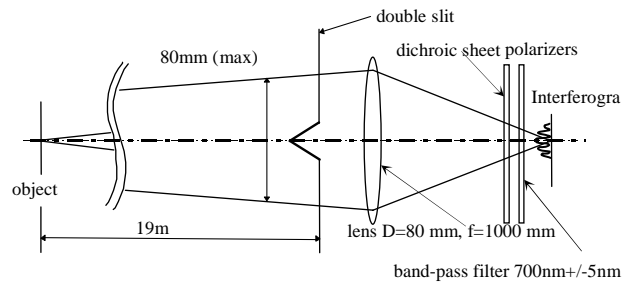


Figure 19  
Aplanatic Fizeau type double-slit SR interferometer for the horizontal beam size measurement.

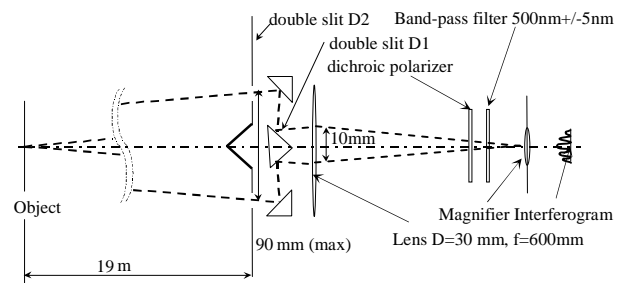


Figure 20  
Nonaplanatic Michelson type SR interferometer for vertical beam size measurement.

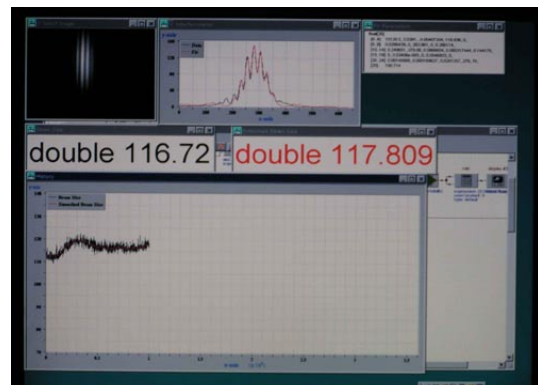


Figure 21  
Display panel for automatic measurement for vertical beam size.

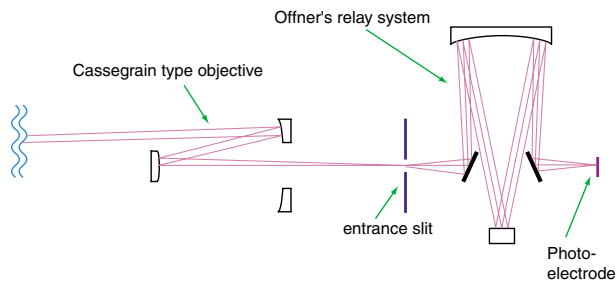


Figure 22  
Incident optics designed based on reflective optics.



Figure 23  
Photograph of the Offner-type relay system with the streak camera. The cover of the Offner-type relay system is opened to show the inside.

graphs are shown in the panel.

In the time-domain measurement using the streak camera, it is important to design an incidence optical system which has an optical path difference (OPD) as small as possible. Because we need an intense light pulse for the streak camera, we prefer to avoid using a band-pass filter, and instead use white light. For this reason, we designed incident optics using reflective optics which has no chromatic aberration as illustrated in Fig. 22. The Cassegrain type objective [5] makes an image of the beam on the entrance slit of the second stage. The light sampled at the entrance slit is then relayed onto the photo electrode of the streak camera by an Offner-type relay system [5]. A photograph of the Offner-type relay system with the streak camera is shown in Fig. 23.

## References

- [1] T. Mitsuhashi and M. Katoh, *Proc. 5th European Particle Accelerator Conference*, p.1669, (1996), Sitges (Barcelona).
- [2] I. Ghozeil "Hartmann and other screen tests" in *Optical shop testing*, Ed. By D. Malacara ,pp367-396,Wiley-International (1992).
- [3] T. Mitsuhashi, "Beam Profile and Size Measurement by SR Interferometer" in *Beam measurement*, Ed. by S. Kurokawa *et al.*, pp399-427, World Scientific(1999).
- [4] J.W. Flanagan, S. Hiramatsu and T. Mitsuhashi, *Proc. 7th European Particle Accelerator Conference*, 1714, (2000), Vienna (Austria).
- [5] L. Mertz, *"Excursions in Astronomical Optics"*, 1996, Springer.

## 3-10 Two New In-Vacuum Type Undulators

In these years we have constructed two new in-vacuum type undulators (U#NW2 and U#NW12) for the PF-AR using a tilt mechanism on the magnet arrays. The construction of U#NW2 was reported before (see Photon Factory Activity Report #18 and #19). U#NW12 has been completed and installed in the PF-AR during this fiscal year. The tilt mechanism has been devised and developed to satisfy the user's two-fold requirements. One is for a very sharp spectrum that is suitable for ordinary diffraction experiments in the hard X-ray region and the other is for a relatively wide spectrum (some 10% relative bandwidth) for XAFS experiments, for example.

In the construction of these undulators, we have employed pure Halbach type magnet arrangements with a period length of 4 cm and number of periods 90 (for U#NW2) and 95 (U#NW12). The selection of the period length was made to cover a photon energy region from 5 keV to 25 keV with the higher harmonics (up to 5th) with 6.5-GeV operation of the PF-AR. Taper of up to  $\pm 2$  mm is allowed for mechanically in the present construction in terms of the difference in the gap size at the entrance and at the exit of the undulator.

Table 2 shows the result of the magnetic adjustments in terms of the ratio of the real brilliance to the ideal case at a magnet gap of 20 mm. The real brilliance corresponds to the real undulator field, and is calculated by direct Fourier Transformation. We find that the state of the undulator field is very fine to produce satisfactorily high brilliance ratios up to 5th harmonic.

The surfaces of the magnets, made of a porous material (NdFeB), are sealed by a TiN coating. The vacuum chamber (of 200 liters capacity) which contains the magnet arrays is evacuated down to  $1 \times 10^{-8}$  Pa using nonevaporable getter (NEG) pumps (4000 l/s for U#NW2 and 5000 l/s U#NW12) and sputter ion pumps (240 l/s for U#NW2 and 480 l/s U#NW12) after the vacuum bakeout at 120°C. In order to avoid the high-temperature deterioration of the magnets during the bake-out process, the magnets were pre-baked at 145°C after magnetization.

Table 2 Comparison of the spectral intensity due to real undulator field to the ideal field at a magnet gap of 20 mm.

	U#NW2	U#NW12
K ( $B_0$ )	1.378 (3690 G)	1.344 (3599 G)
1 <sup>st</sup> harmonic photon energy	5145 eV	5270 eV
Brilliance ratio		
1 <sup>st</sup> harmonic	100 %	100 %
3 <sup>rd</sup> harmonic	91 %	96 %
5 <sup>th</sup> harmonic	81 %	90 %